

Druitt, T.H., Kutterolf, S., Ronge, T.A., and the Expedition 398 Scientists *Proceedings of the International Ocean Discovery Program* Volume 398 publications.iodp.org







Site U1597¹

Contents

- 1 Background and objectives
- 2 Operations
- 3 Lithostratigraphy
- 8 Stratigraphic correlation
- 8 Structural geology
- 8 Biostratigraphy
- 9 Paleomagnetism
- Pl
- 9 Physical properties
- 11 Geochemistry
- 14 References

Keywords

International Ocean Discovery Program, IODP, R/V JOIDES Resolution, Expedition 398, Hellenic Arc Volcanic Field, Earth Connections, Earth in Motion, Biosphere Frontiers, Site U1597, Santorini caldera, Aegean Sea, Christiana-Santorini-Kolumbo volcanic field, subduction zone, shallow-marine volcanism

Core descriptions

Supplementary material

References (RIS)

MS 398-111

Published 30 July 2024

Funded by NSF OCE1326927, ECORD, and JAMSTEC

T.H. Druitt, S. Kutterolf, T.A. Ronge, S. Beethe, A. Bernard, C. Berthod, H. Chen, S. Chiyonobu, A. Clark, S. DeBari, T.I. Fernandez Perez, R. Gertisser, C. Hübscher, R.M. Johnston, C. Jones, K.B. Joshi, G. Kletetschka, O. Koukousioura, X. Li, M. Manga, M. McCanta, I. McIntosh, A. Morris, P. Nomikou, K. Pank, A. Peccia, P.N. Polymenakou, J. Preine, M. Tominaga, A. Woodhouse, and Y. Yamamoto²

¹ Druitt, T.H., Kutterolf, S., Ronge, T.A., Beethe, S., Bernard, A., Berthod, C., Chen, H., Chiyonobu, S., Clark, A., DeBari, S., Fernandez Perez, T.I., Gertisser, R., Hübscher, C., Johnston, R.M., Jones, C., Joshi, K.B., Kletetschka, G., Koukousioura, O., Li, X., Manga, M., McCanta, M., McIntosh, I., Morris, A., Nomikou, P., Pank, K., Peccia, A., Polymenakou, P.N., Preine, J., Tominaga, M., Woodhouse, A., and Yamamoto, Y., 2024. Site U1597. In Druitt, T.H., Kutterolf, S., Ronge, T.A., and the Expedition 398 Scientists, Hellenic Arc Volcanic Field. Proceedings of the International Ocean Discovery Program, 398: College Station, TX (International Ocean Discovery Program). https://doi.org/10.14379/iodp.proc.398.111.2024

² Expedition 398 Scientists' affiliations.

Background and objectives

Site U1597 (proposed Site CSK-05C) is located in the northern basin of the Santorini caldera (Figure **F1**). It lies at a water depth of 382 meters below sea level (mbsl) and has a maximum recovery depth of 42.7 meters below seafloor (mbsf) (all depths below seafloor are given using the core depth below seafloor, Method A [CSF-A], scale, except in **Operations** where the drilling depth below seafloor [DSF] scale is used) with 94% core recovery. Site U1597 addresses the same drilling objectives and lies southeast of Site U1596. Two additional sites (U1594 and U1595) lie in the southern caldera basin.

Four seismic units have been recognized in the Santorini caldera (Johnston et al., 2015; Nomikou et al., 2016) (Figure **F2**). They were thought to consist of muds and sands from cliff mass wasting (Unit S1); compacted (possibly lithified) sandy volcaniclastics from Kameni Volcano (Unit S2); and consolidated coarse blocky intracaldera tuffs, landslide debris, and/or flood gravels (Unit S3). Seis-

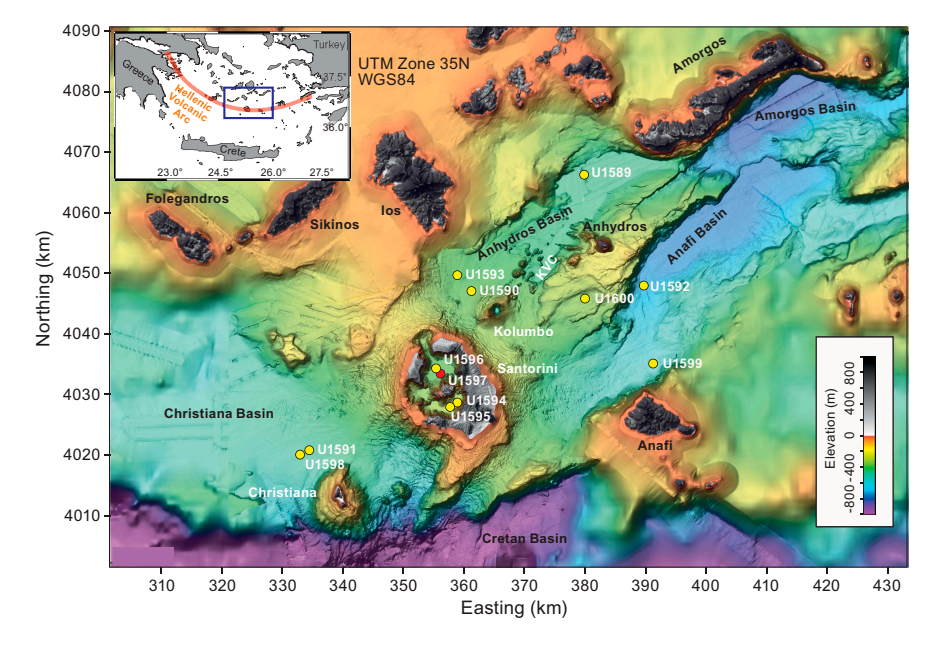


Figure F1. Site map. Red = Site U1597, yellow = other sites. Inset: location map. See Figure F1 in the Site U1589 chapter (Druitt et al., 2024) for citations for the swath data on which this map is based. KVC = Kolumbo volcanic chain.

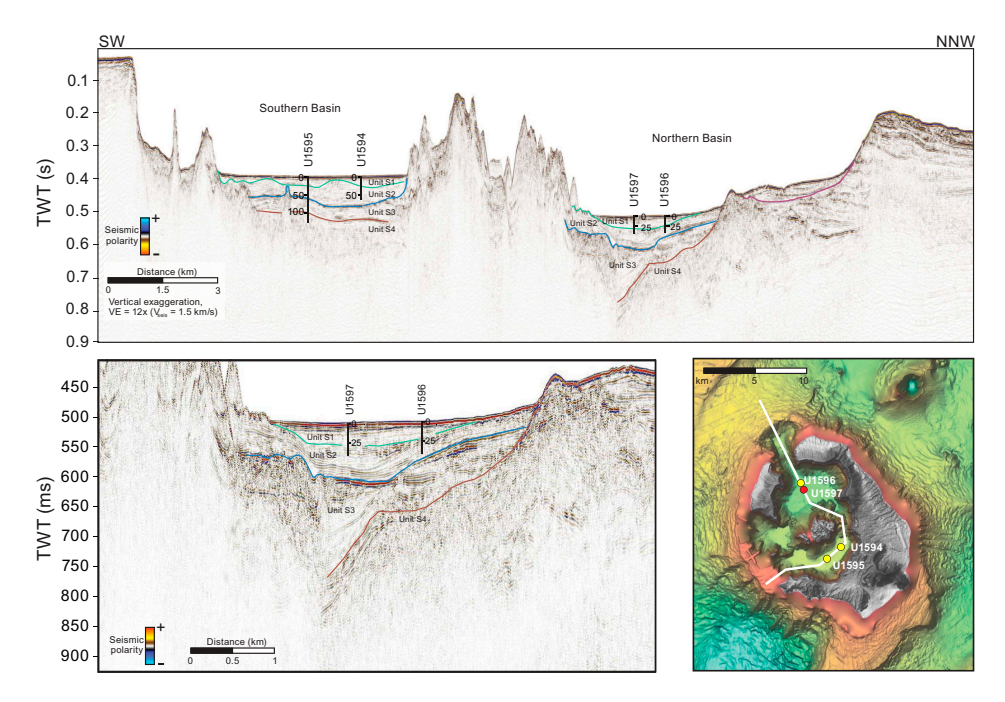


Figure F2. Top: seismic profile across the Santorini caldera with Seismic Units S1–S4, Sites U1594–U1597. Depths in meters. TWT = two-way traveltime. Bottom left: profile of Sites U1596 and U1597. Right: locations of the four intracaldera sites. Red = Site U1597, yellow = other sites.

mic Unit S4 was thought to be intracaldera tuff from the Late Bronze Age eruption. The four caldera sites were planned to sample Units S1–S3; test the published correlations between the two caldera basins; penetrate below Unit S3 into Unit S4; and address scientific Objectives 1, 4, 5, and 7 of the Expedition 398 Scientific Prospectus (Druitt et al., 2022). By drilling both caldera basins and exploiting our dense seismic reflection coverage, we gained access to the 3D architecture of the entire caldera fill. We also addressed the question of why the northern basin is 100 m deeper than the southern one, with a thicker Unit S1 but a thinner Unit S3. Finally, we tested whether Unit S3 consisted of flood debris from the caldera-flooding event (Nomikou et al., 2016) or whether it was Late Bronze Age intracaldera tuff (Johnston et al., 2015). The intracaldera sites were used for microbiological work of Objective 7.

2. Operations

The revised plan for Site U1597 was to keep the drilling operations very conservative while learning the nature of the formation to aid in planning future caldera work. The immediate foreseen work was limited to 1-2 holes, each 40-50 mbsf deep.

2.1. Hole U1597A

Hole U1597A (36°26.2494′N, 05°22.7326′E) was spudded on 24 January 2023 at 1240 h. With a recovery of 5.6 m, the seafloor depth was calculated as 382.3 mbsl (Table **T1**). Coring continued with the advanced piston corer (APC) system through Core 5H to a final depth of 43.6 mbsf. Again, excessive torque started building.

The drill string was tripped up with the top drive, and the bit cleared the seafloor at 1547 h. The bit cleared the rotary table at 1728 h.

The floor was secured for transit. The thrusters were raised starting at 1815 h. The vessel was switched to bridge control at 1818 h. All thrusters were up and secure, and the start of the sea passage began at 1824 h, ending Site U1597.

Table T1. Core summary, Site U1597. mbsf = meters below seafloor. NA = not applicable. DSF = drilling depth below seafloor. H = APC. **Download table in CSV format.**

Hole U1597A

Latitude: 36°26.2494′N Longitude: 25°22.7326′E Water depth (m): 382.35

Date started (UTC): 0930 h; 24 January 2023

Date finished (UTC): 1630 h; 24 January 2023

Time on hole (days): 0.29 Penetration (mbsf): 43.6 Cored interval (m): 43.6 Recovered length (m): 40.84 Recovery (%): 93.67

Drilled interval (m): NA
Drilled interval (no.): 0

Drilled interval (no.): Total cores (no.): 5

APC cores (no.): 5

Core	Top depth drilled DSF (m)	Bottom depth drilled DSF (m)	Interval advanced (m)	Recovered length (m)	Core recovery (%)	Core on deck date (2023)	Core on deck time UTC (h)
398-U1	597A-						
1H	0.0	5.6	5.6	5.63	101	24 Jan	1055
2H	5.6	15.1	9.5	9.64	101	24 Jan	1130
3H	15.1	24.6	9.5	8.86	93	24 Jan	1155
4H	24.6	34.1	9.5	8.19	86	24 Jan	1220
5H	34.1	43.6	9.5	8.52	90	24 Jan	1250
		Totals:	43.6	40.84	-		

3. Lithostratigraphy

Cores from Site U1597 recovered a coherent stratigraphy from 0 to 42.62 mbsf (Sections 398-U1597A-1H-1 through 5H-CC) (Figure F3). Only one hole (U1597A) was drilled at this site.

The recovered material is unlithified sediment dominated by volcanic material with minor amounts of mud and tuffaceous mud in the uppermost 8 m. Smear slides for microscopic analyses were prepared to confirm macroscopic descriptions of distinct lithology changes at the core section level, such as identification of vitric ash particles in tuffaceous lithologies or crystals in ash layers. X-ray diffraction (XRD) data were obtained from three interstitial water (IW) squeeze cake sediment residues from Hole U1597A.

Figure F3 summarizes the lithostratigraphy of Site U1597, displaying core recovery and the lithostratigraphic unit and subunits. Table T2 provides the upper and lower boundaries, thicknesses, biostratigraphic ages (see Biostratigraphy), and lithologic summary of the unit and subunits. Figure F4 graphically presents the relative proportions of volcanic, tuffaceous, and nonvolcanic lithologies in Hole U1597A, with the lithostratigraphic unit and subunits labeled. Figure F5 presents the schematic grain size distribution of the sediments, in particular the changes in grain size within the volcanic-dominated unit, to graphically show the distribution of ash, lapilli-ash, and lapilli. Figure F6 displays different types of core disturbance observed at the site.

The following sections describe (1) the effects of core disturbance, (2) the lithostratigraphic unit and subunits, and (3) XRD data results from Site U1597.

3.1. Core disturbance

Site U1597 is affected by two types of core disturbance:

- Soupy: typically restricted to water-saturated intervals of unconsolidated ash, overprinting original sedimentary or depositional structures (Figure F6A).
- Artificial size and density segregation: likely to occur during drilling or with postrecovery core handling processes on board (e.g., inclining, shaking, and plunging cores on the catwalk to compact sediments). Jutzeler et al. (2014) also described pseudohorizontal density grading that

can occur while the core is lying flat on deck, resulting in vertical structures once the core is turned upright. Such core disturbance is observed most often in volcanic sediments because increased porosity allows sucking in of seawater during hydraulic piston coring. The resulting soupy texture allows material to flow within the core liner. Secondary normal or reverse grading, or density separation of clasts, may occur as a result of this disturbance and obscure primary sedimentary features (Figure F6B).

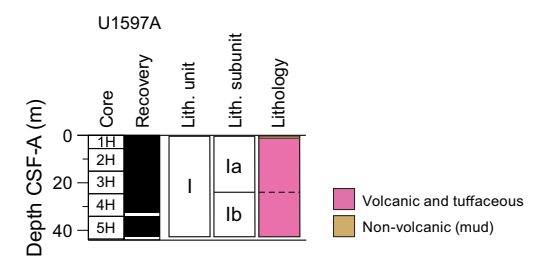


Figure F3. Lithostratigraphy, Site U1597. The nonvolcanic mud lies at the top of interval 1H-1, 0–6 cm. Unit color = dominant lithology.

Table T2. Lithostratigraphic unit and subunits, Hole U1597A. * = bottom not recovered, end of hole. Download table in CSV format.

Lith. unit	Subunit	Top depth (mbsf)	Top core, section, interval (cm)	Bottom depth (mbsf)	Bottom core, section, interval (cm)	Thickness (m)	Stratigraphic age	Lithologic summary
1	la Ib	0.00 24.60	398-U1597A- 1H-1, 0 4H-1, 0	23.96 42.62*	398-U1597A- 3H-CC, 17 5H-CC, 11	23.96 >18.02	Holocene	Massive, fine grained, dark gray ash with minor intervals of mud or tuffaceous mud Massive, dark gray to gray lapilli-ash and lapilli

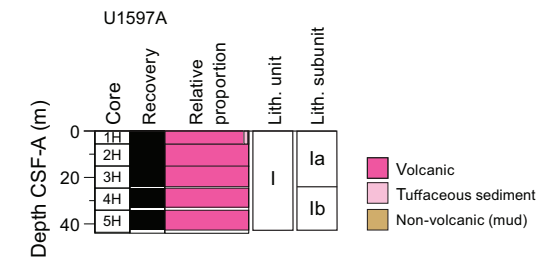


Figure F4. Relative percentages of volcanic, tuffaceous, and nonvolcanic lithologies, Site U1597. Unit I is volcanic dominated.

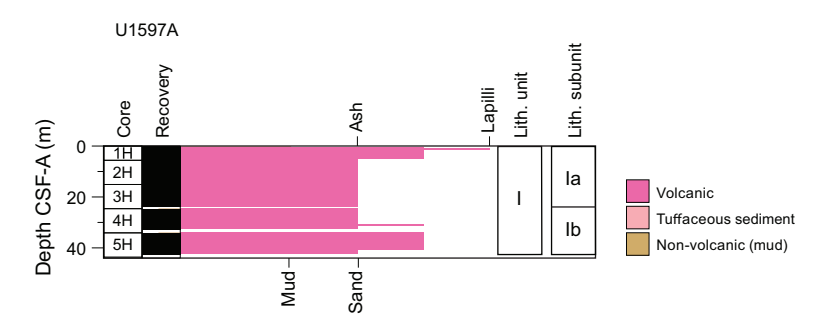


Figure F5. Grain size distributions of volcanic, tuffaceous, and nonvolcanic sediments, Site U1597. Length of colored bars = relative grain size (ash = <2 mm, lapilli = 2-64 mm, mud = <63 μ m, sand = 0.063-2 mm), with separate scales shown for volcanic grain size (top) and nonvolcanic grain size (bottom, used for tuffaceous and nonvolcanic sediments). Mixed lithologies such as lapilli-ash (dark pink) that have relative grain sizes between two categories are plotted between ticks.

3.2. Description of unit and subunits

3.2.1. Unit I

Interval: 398-U1597A-1H-1, 0 cm, to 5H-CC, 11 cm (bottom of the hole)

Depth: 0.00–42.62 mbsf Thickness: >42.62 m Age: Holocene

Lithology: volcanic (ash, lapilli, and lapilli-ash) and minor tuffaceous lithologies (tuffaceous mud) and nonvolcanic sediment (mud)

Unit I extends from 0 to 42.62 mbsf in Hole U1597A (Table T2) and consists of a fine- to coarse-grained dark gray ash sequence in the uppermost ~15 m, partly accompanied by lapilli-sized clasts, and a slightly lighter colored ash and lapilli-ash interval that continues for the remainder of Hole U1597A. One interval of 27 cm thick tuffaceous mud is observed within the upper section (398-U1597A-1H-1).

Volcanic lithologies (>75% volcanic particles; glass shards, pumice, and crystals) comprise ash, lapilli-ash, and lapilli, based on the relative abundance of ash-sized (<2 mm) and lapilli-sized (2–64 mm) particles, as described in **Lithostratigraphy** in the Expedition 398 methods chapter (Kutterolf et al., 2024). Ash and lapilli were used when the proportion of one size was >75%, and lapilli-ash was described when both grain sizes were present but at <75% abundance (Fisher and Schmincke, 1984).

Subunits in Unit I were defined by changes in grain size, color, and componentry and are described as follows (Figures **F3**, **F4**, **F5**; Table **T2**):

- Subunit Ia (Sections 398-U1597A-1H-1, 0 cm, through 3H-CC, 17 cm; 0–23.96 mbsf): fine- to coarse-grained dark gray ash and lapilli-ash with minor intervals of lapilli, mud, or tuffaceous mud.
- Subunit Ib (Sections 398-U1597A-4H-1, 0 cm, through 5H-CC, 11 cm; 24.6–42.62 mbsf): dark gray fine- to coarse-grained ash and lapilli-ash.

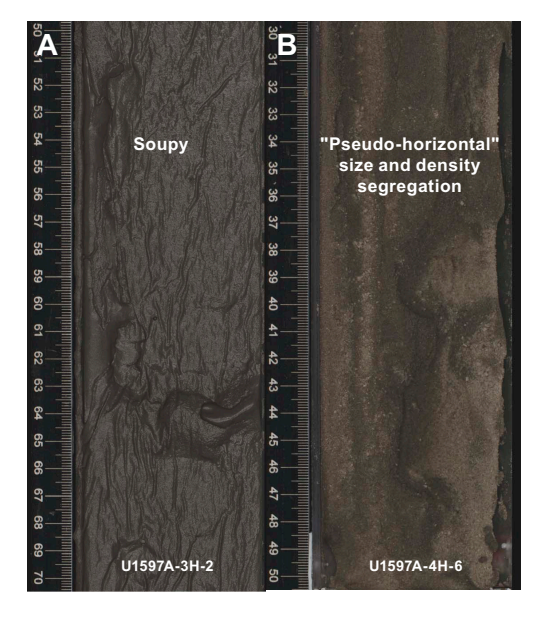


Figure F6. Core disturbances, Site U1597. A. Soupy ash. B. Artificial size and density grading or pseudohorizontal density grading caused by segregation of fine lapilli pumice clasts in liquefied sediments while the core is lying flat on the deck, resulting in vertical structures when the core is turned upright.

3.2.1.1. Subunit la

Subunit Ia extends from 0 to 23.96 mbsf in Hole U1597A (Sections 1H-1, 0 cm, through 3H-CC, 17 cm) (Figure F3; Table T2). This subunit consists predominantly of volcanic lithologies (ash, lapilliash, and lapilli) (Figure F7) with minor amounts of tuffaceous sediment (tuffaceous mud) and nonvolcanic sediment (mud) in the uppermost section. The uppermost interval of Subunit Ia is a ~6 cm thick brown mud, followed by ~25 cm of gray tuffaceous mud. Farther downcore, intervals of ash, lapilliash, and lapilli occur, dominated by a well-sorted gray to dark grayish brown to greenish black ash sequence (Figure F7B). In Core 1H, coarse-grained volcanic intervals are composed of poorly sorted gray lapilliash and lapilli, with maximum grain sizes varying between fine and coarse lapilli (Figure F7A). Pumice clasts are commonly subangular and white and dark gray. Some clasts have mafic enclaves or are banded. The color of the ash ranges from greenish black in the upper part (Figure F7B) to very dark grayish brown in the lower part (Figure F7C).

3.2.1.2. Subunit Ib

Subunit Ib extends from 24.6 to 42.62 mbsf in Hole U1597A (Sections 4H-1, 0 cm, through 5H-CC, 11 cm) (Figure F3; Table T2). The total thickness of this subunit is >18 m and consists of ash and lapilli-ash (Figure F8). The bottom of the unit was not recovered due to termination of drilling. The top of Subunit Ib is recognized by a distinct color change from very dark grayish brown volcanic ash, characteristic for Subunit Ia, to dark gray volcanic ash and lapilli-ash, characteristic for Subunit Ib. This boundary coincides with an increase in scattering of *P*-wave velocities (see **Physical properties**). The upper part of Subunit Ib is ash dominated (Figure F8A), with grain size variations from fine ash to coarse ash and maximum grain sizes of medium to coarse lapilli. Farther down in the core, the sediments transition into lapilli-ash (Figure F8B, F8C) between 34.1 and 41.05 mbsf (Figure F8C).

Intervals of ash are typically dark gray and characterized by well-sorted grain sizes ranging from fine to coarse ash. Minor amounts of dispersed banded, white, and gray subangular pumice lapilli

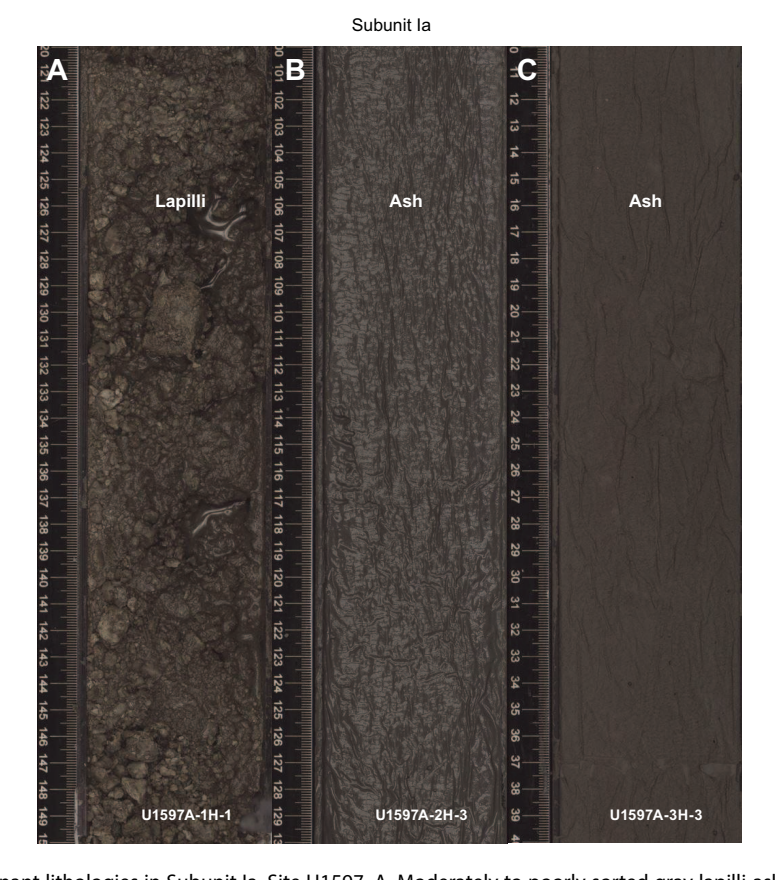


Figure F7. Dominant lithologies in Subunit Ia, Site U1597. A. Moderately to poorly sorted gray lapilli-ash observed in the uppermost core section. (B) Greenish dark and (C) very dark grayish brown ash intervals.

occur in most ash intervals. Lapilli-ash intervals are also dark gray and consist of subangular pumice lapilli (Figure F8B, F8C). These are typically white or gray and have a vesicular to highly vesicular texture with vesicle shapes ranging from elongated to tubular. Banded pumices, characterized by dark-colored bands in light-colored or brown pumice, and small mafic enclaves are common in some intervals. Plant fragments are observed at ~40 m in interval 398-U1597A-5H-5, 0–93 cm. Hole U1597A ends in dark and well-sorted coarse ash with small amounts of white and dark gray pumices (Figure F8D).

3.3. X-ray diffraction

XRD data were collected from three IW squeeze cake sediment residues from Hole U1597A. The analyzed samples are volcanic lithologies (ash) from Subunit Ia only. XRD spectra of these three ash samples are shown in Figure $\mathbf{F9}$. The volcanic ash samples from Hole U1597A show a characteristic hump at low °20, indicating the presence of volcanic glass. The only identified crystalline phases in the ash samples are Ca-rich plagioclase, clay minerals of the illite group, and zeolite.

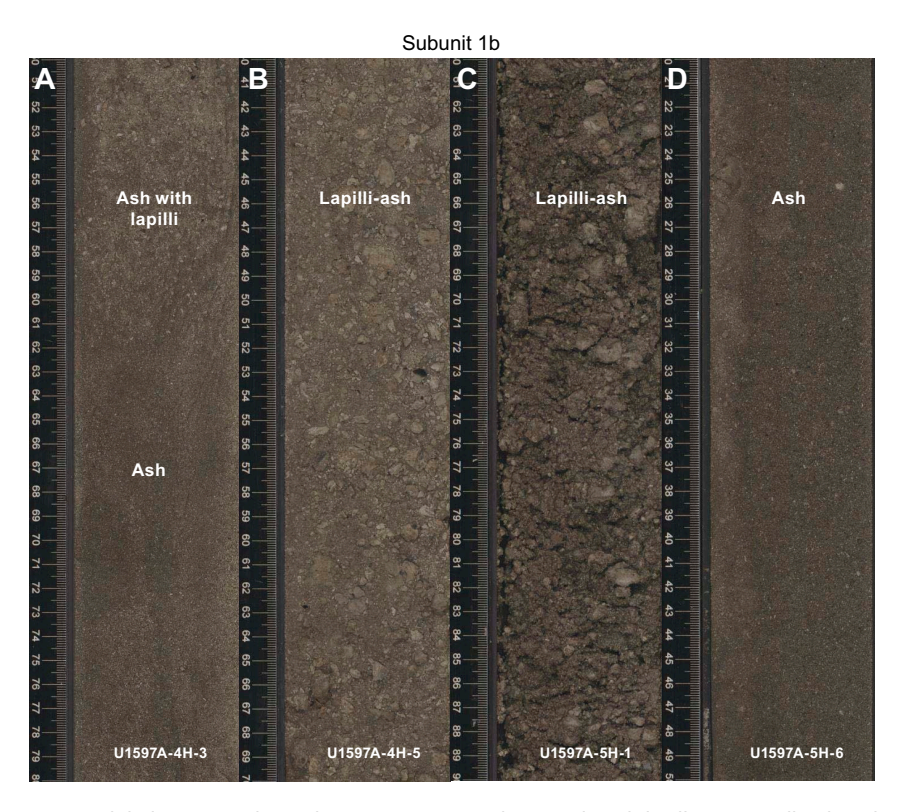


Figure F8. Dominant lithologies in Subunit Ib, Site U1597. A. Dark gray ash with lapilli. B, C. Lapilli-ash with subangular white, gray, and banded pumice. D. Ash intervals.

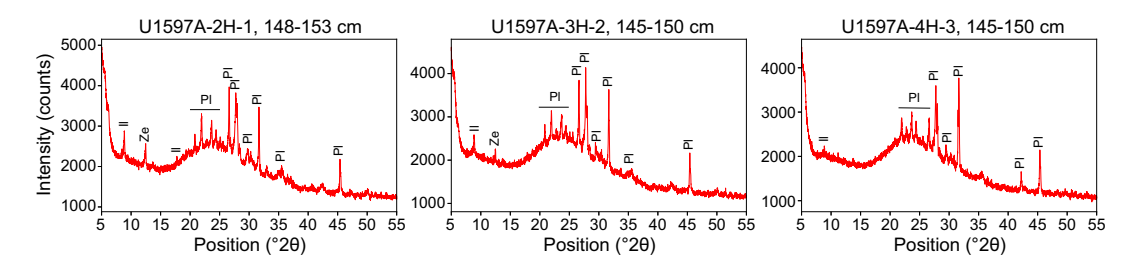


Figure F9. Selected XRD spectra of Subunit la volcanic lithologies (ash), Site U1597. Samples show a characteristic hump at low °2θ, indicating the presence of volcanic glass. Identified crystalline phases are Ca-rich plagioclase, clay minerals typical of the illite group, and zeolite. II = illite, Ze = zeolite, PI = Ca-rich plagioclase.

4. Stratigraphic correlation

Because only one hole was drilled at Site U1597, no stratigraphic correlation could be made.

5. Structural geology

It was not possible to measure orientations of structures at Site U1597. Although there were some bedding planes, core-induced disturbance prevented their measurement.

6. Biostratigraphy

Planktonic and benthic foraminifera and calcareous nannofossils were examined from core catcher samples from Hole U1597A to assess the paleoenvironmental conditions of Site U1597.

Site U1597 cored the sedimentary sequence in the northeast portion of the Santorini caldera and recovered a 42.62 m thick sequence composed primarily of volcanogenic sediments. No calcareous nannofossils or benthic foraminifera were found in core catcher samples; however, very rare, moderately preserved planktonic foraminifera were found in Samples 398-U1597A-2H-CC, 10–15 cm, and 5H-CC, 11–16 cm (Table T3), in the form of *Globoturborotalita rubescens* (Figure F10) and *Globigerinoides ruber*, respectively. Additionally, rare Ostracoda were found in Sample 1H-CC, 6–13 cm, although biological remains were of insufficient quantity to permit paleoenvironmental analyses.

Table T3. Distribution of planktonic foraminifera, Site U1597. Download table in CSV format.

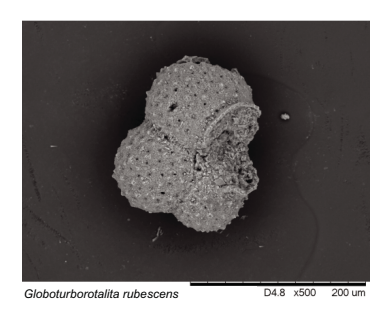


Figure F10. Planktonic foraminifer. Globoturborotalita rubescens (398-U1597A-1H-CC, 6–13 cm).

7. Paleomagnetism

None of the cores recovered at Site U1597 were suitable for paleomagnetic analysis.

8. Physical properties

At Site U1597, approximately 20% of discrete samples have grain densities <2.0 g/cm³. Thermal conductivity is lower than typical values for sediments at similar depths.

8.1. Whole-round GRA density, MS, P-wave velocity, and NGR

Figure **F11** summarizes data collected on whole-round cores measured on the gamma ray attenuation (GRA) densitometer, magnetic susceptibility (MS) loop, and *P*-wave velocity logger on the Whole-Round Multisensor Logger (WRMSL) as well as natural gamma radiation (NGR). All cited depths are on the CSF-A scale. Some systematic sources of error were noted in the data measured on the unconsolidated volcaniclastic-rich Hole U1597A formation that should be considered when interpreting absolute values and trends:

- Redistribution of unconsolidated volcaniclastic materials in core liners during coring and on the core retrieving platform can lead to sorting by particle size and density.
- Core liners sometimes contained large amounts of water. As a result, WRMSL measurements of bulk density are systematically lower than discrete measurements at this site.
- Measured physical properties values can therefore change. Whole-round measurements in sections that match discrete measurement values on split cores are thus most reliable.

The layer at 1–5 mbsf has distinctly higher *P*-wave velocity and lower bulk density than volcaniclastic deposits at shallower and greater depths. Overall, there is a general trend of decreasing NGR with increasing depth. Otherwise, the cored depth range is too small to identify clear trends with depth.

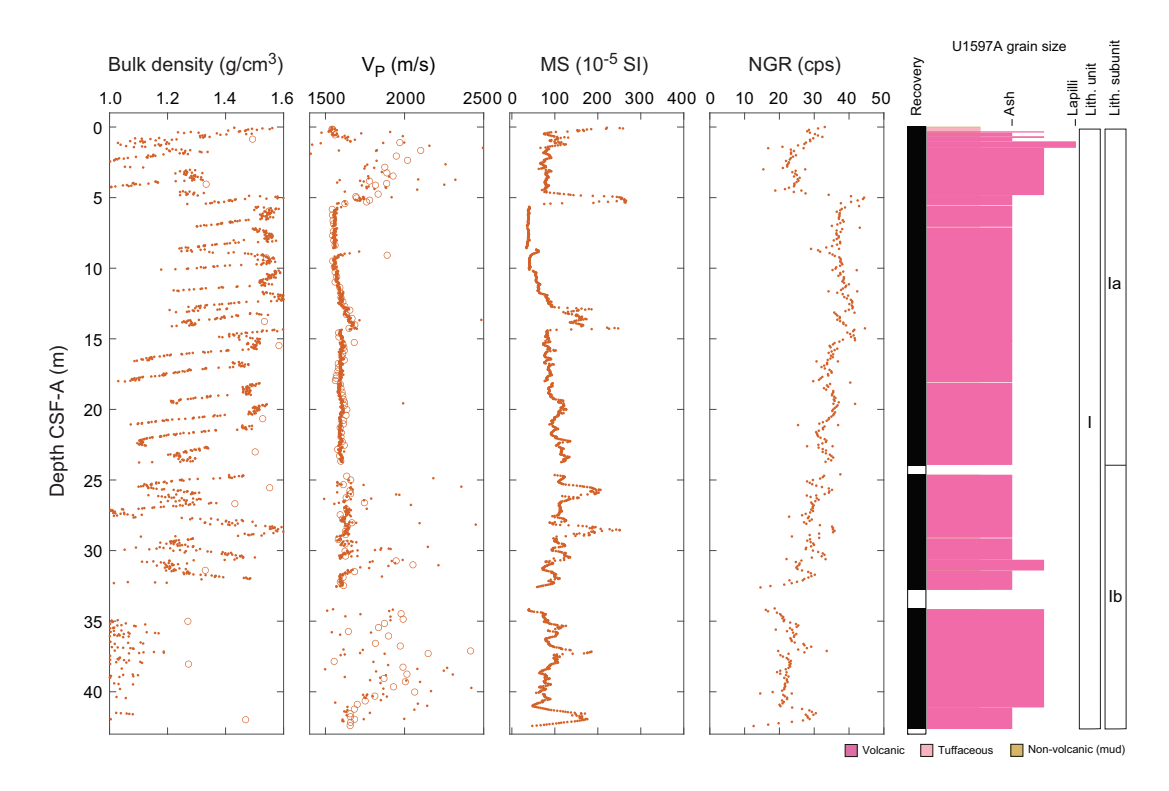


Figure F11. Physical properties, Site U1597. Dots = whole-round measurements, open symbols = discrete measurements. cps = counts per second.

8.2. Discrete measurements

8.2.1. Material strength

A total of seven automated vane shear (AVS) strength measurements were made on selected working-half sections. Because volcaniclastic materials are not suitable for these measurements, few measurements could be made (Figure **F12**; Table **T4**).

8.2.2. P-wave velocity

A total of 127 *P*-wave velocity measurements were conducted on working-half sections (Figure **F12**; Table **T5**). Discrete measurements of *P*-wave velocity on working-half sections are similar to those measured using the WRMSL on whole-round cores (Figure **F11**). A high *P*-wave velocity layer with low bulk density exists between 1 and 5 mbsf. The large scatter below 30 mbsf arises from a combination of measurements that capture bulk sediment properties (lower values) and measurements made across a small number of lapilli clasts (larger values). For lapilli and larger sized clasts, the particle size was a substantial fraction of the distance between the two calipers used to make the measurements; hence, the measurements may not be representative of true bulk properties (i.e., sample size is not much larger than a representative elementary volume).

8.2.3. Moisture and density

A total of 14 discrete samples were collected for moisture and density (MAD) measurements (Figure F12; Table T6). Bulk density derived by MAD measurements on discrete samples should be more reliable than GRA data from WRMSL on whole-round cores, although in both cases, coring and recovery disturbances may have impacted measured values.

Porosity ranges 58-70 vol% (mean = 65 vol%; standard deviation = 4 vol%). Bulk density ranges 1.3-1.6 g/cm³ (mean = 1.46 g/cm³). Bulk density does not obviously increase with depth.

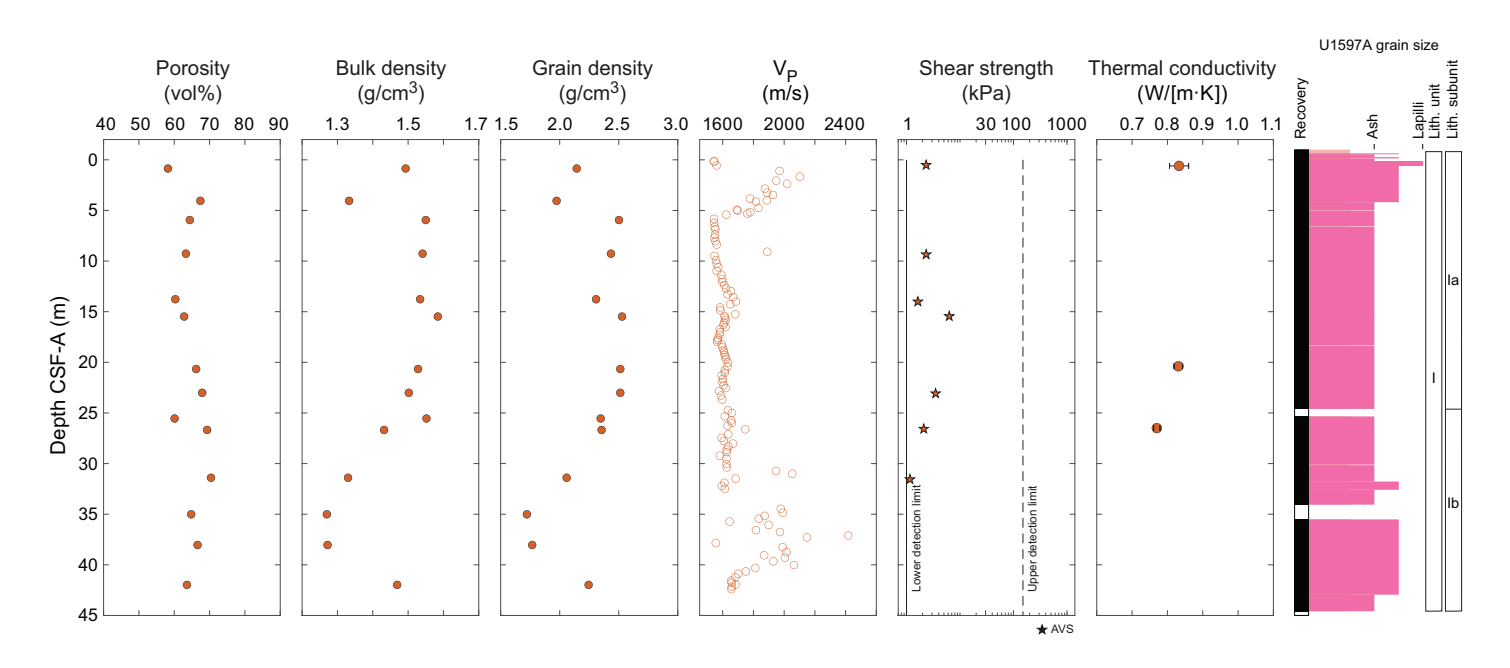


Figure F12. Discrete physical properties measurements, Site U1597. Dashed line = AVS upper measurement limit, solid line = AVS lower measurement limit.

Table T4. Shear strength, Site U1597. Download table in CSV format.

Table T5. P-wave velocity, Site U1597. Download table in CSV format.

Table T6. MAD measurements, Site U1597. Download table in CSV format.

Table T7. Thermal conductivity measurements, Site U1597. Download table in CSV format.

Grain density ranges $1.7-2.5 \text{ g/cm}^3$ (mean = 2.24 g/cm^3 ; median = 2.3 g/cm^3). A total of 21% of discrete samples have grain densities $<2.0 \text{ g/cm}^3$; grain density decreases with increasing depth.

8.2.4. Thermal conductivity

Three thermal conductivity measurements were made on selected working-half sections (Table T7; Figure F12). Measurements could not be made on coarse volcaniclastic materials; hence, the values we report are not representative of the full range of recovered lithologies. Compared to typical sediments in which thermal conductivity is close to 1 W/(m·K) at these depths below seafloor, the mean value of 0.81 W/(m·K) is low in volcaniclastic sediments at Site U1597.

9. Geochemistry

9.1. Volcaniclastic bulk geochemistry

To determine the geochemistry of the volcanic and tuffaceous materials, three tephra samples were handpicked from various layers in Hole U1597A. Following cleaning, grinding, fusion, and dissolution, the materials were analyzed shipboard for major (Si, Al, Fe, Mg, and Ca), minor (Ti, Mn, Na, K, and P), and trace (Sc, V, Cr, Co, Ni, Cu, Zn, Rb, Sr, Y, Zr, Nb, Ba, Ce, and Nd) elements using inductively coupled plasma—atomic emission spectroscopy (ICP-AES) (see **Geochemistry** in the Expedition 398 methods chapter [Kutterolf et al., 2024] for analytical technique). Several unknown samples were run multiple times to determine analytical reproducibility.

9.1.1. ICP-AES: major, minor, and trace elements

All of the volcaniclastic units sampled were classified as dacites or trachydacites (Table **T8**; Figure **F13**). Bulk chemistry values are less evolved than glass chemistry reported in Kutterolf et al. (2021), as expected due to bulk analyses including both minerals and glass.

Concentrations are reported for all analyzed trace elements, but Ce, Cr, Cu, Nb, Ni, P, Rb, S, and V were below detection limits in the majority of samples and are not shown for respective samples in Table **T8**; volcaniclastic analytical errors are $\pm 1\%$ for major elements and $\pm 5\%$ –10% for trace elements (see **Geochemistry** in the Expedition 398 methods chapter [Kutterolf et al., 2024]). Trace element ratios were used to broadly discriminate between the volcanic centers of Kolumbo, Santorini, and Christiana.

9.2. Interstitial water geochemistry

To determine the inorganic constituents of IW, a total of five water samples were taken from the mudline and whole-round squeezing of sediment intervals at Site U1597. Aliquots of IW were used for shipboard analyses, and the remaining water was taken for shore-based analysis following protocols specified by individual scientists. The retrieved pore waters were analyzed shipboard for salinity, alkalinity, pH, major anions (Cl⁻, SO₄²⁻, and Br⁻), major cations (Ca²⁺, Na⁺, Mg²⁺, and K⁺), and major (S, Ca, Mg, K, and Na) and minor (B, Ba, Fe, Li, Mn, P, Si, and Sr) elements using the methods described in **Geochemistry** in the Expedition 398 methods chapter (Kutterolf et al., 2024).

9.2.1. Salinity, alkalinity, and pH

Salinity values are 40 throughout Hole U1597A (Table T9; Figure F14). No variations were recorded.

Alkalinity increases (2.4–6.6 mM) with depth to 18.1 mbsf before decreasing again to the base of the hole (Table **T9**; Figure **F14**).

Values for pH show very slight variation within the sampled depths, ranging 7.6–7.7; values increase with depth in IW samples (Table **T9**; Figure **F14**).

9.2.2. Bromide, chloride, boron, sodium, potassium, magnesium, calcium, and sulfate

Bromide, Cl⁻, Na⁺, and Mg²⁺ all increase with depth at Site U1597, whereas B decreases (Table **T10**; Figure **F15**). Potassium and Ca²⁺ are inversely correlated, decreasing to a minimum of 5.7 mM at 18.1 mbsf, whereas Ca²⁺ increases to a maximum of 15 mM at the same depth. Sulfate

Table T8. ICP-AES data for major, minor, and trace elements, Site U1597. Download table in CSV format.

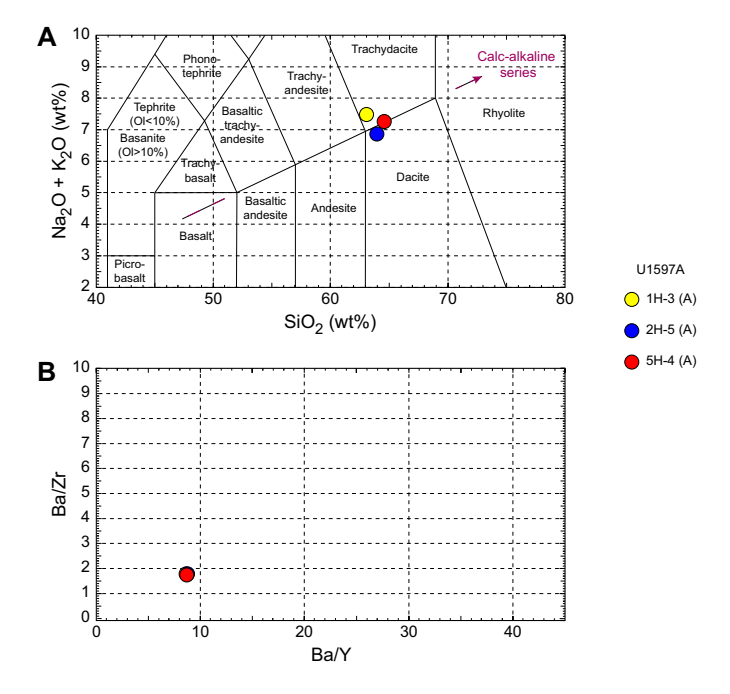


Figure F13. ICP-AES analyses of selected volcaniclastic units used to discriminate between potential volcanic sources, Site U1597. A. Total alkali vs. SiO_2 plot with the rock nomenclature of Le Maitre et al. (2002) overlain used for sample naming. OI = olivine. B. Ba/Y vs. Ba/Zr plot used to correlate samples. Note that all three samples overlap completely in the provided plot.

Table T9. Alkalinity, pH, and salinity values, Site U1597. Download table in CSV format.

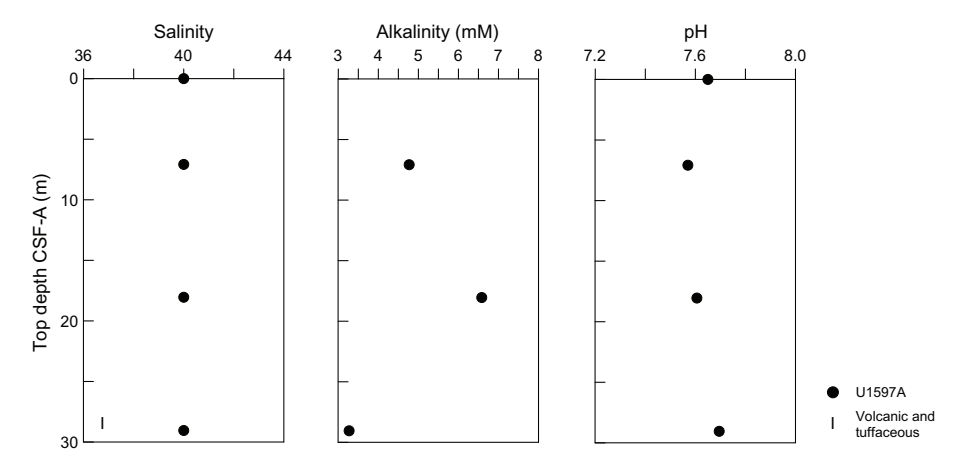


Figure F14. IW salinity, alkalinity, and pH, Site U1597. Lithostratigraphic Unit I is described in Lithostratigraphy.

Table T10. IW data for major anions and cations measured using ion chromatography and major and minor elements measured using ICP-AES, Site U1597. **Download table in CSV format.**

decreases from 33 mM at the mudline to 31.3 mM at 18.1 mbsf before increasing again to 33.4 mM at 29.1 mbsf.

9.2.3. Lithium, iron, manganese, barium, silicon, and strontium

IW values of Li are inversely correlated with Mn, Ba, and Sr, whereas Fe and Si both increase with depth to maxima at 18.1 mbsf before slightly decreasing downhole (Table **T10**; Figure **F16**). The maxima for Fe, Mn, and Si are one order of magnitude higher than surrounding pore fluid values. Phosphorus was only above detection limit in one sample at 7.1 mbsf, which corresponds to the maximum in Mn.

9.3. Sediment bulk geochemistry

Three sediment samples were analyzed for bulk geochemistry (Table **T11**). All were analyzed for total carbon, hydrogen, and nitrogen (CHN) and for inorganic carbon and carbonate content (see **Geochemistry** in the Expedition 398 methods chapter [Kutterolf et al., 2024]). For CHN analysis, duplicates were run for \sim 10% of the samples to determine analytical reproducibility (standard deviation: N = 0.01; C = 0.04). Carbonate values peaked at 0.6 wt% (Table **T11**).

9.3.1. Sapropel identification

Total organic carbon (TOC) was calculated using total carbon and inorganic carbon values. Following the convention set forth by Kidd et al. (1978), units with TOC values >2.0 wt% were identified as sapropels and units with TOC values of 0.5–2.0 wt% were identified as sapropelitic. Using these values, no units were identified as sapropels or sapropelitic (Table **T11**).

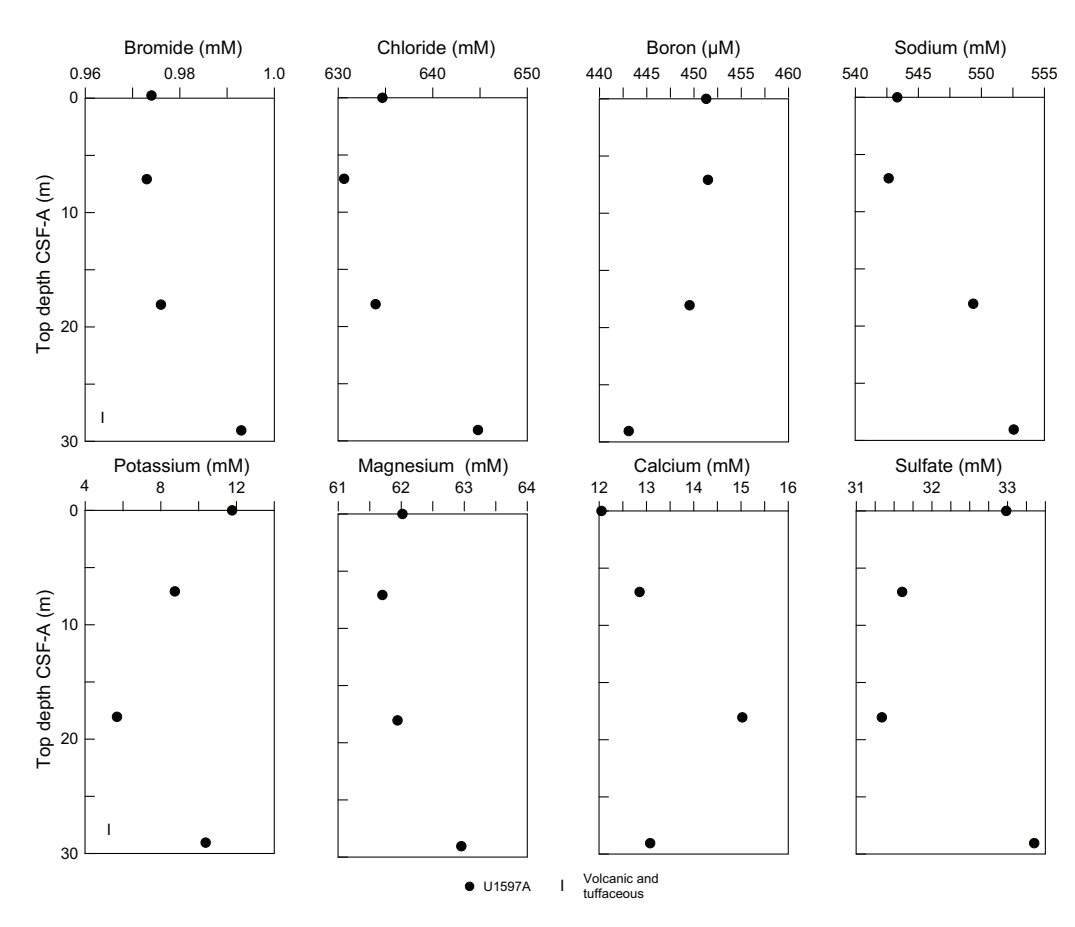


Figure F15. IC and ICP-AES concentrations of Br, Cl, B, Na, K, Mg, Ca, and SO_4^{2-} in IW samples, Site U1597. Lithostratigraphic Unit I is described in Lithostratigraphy.

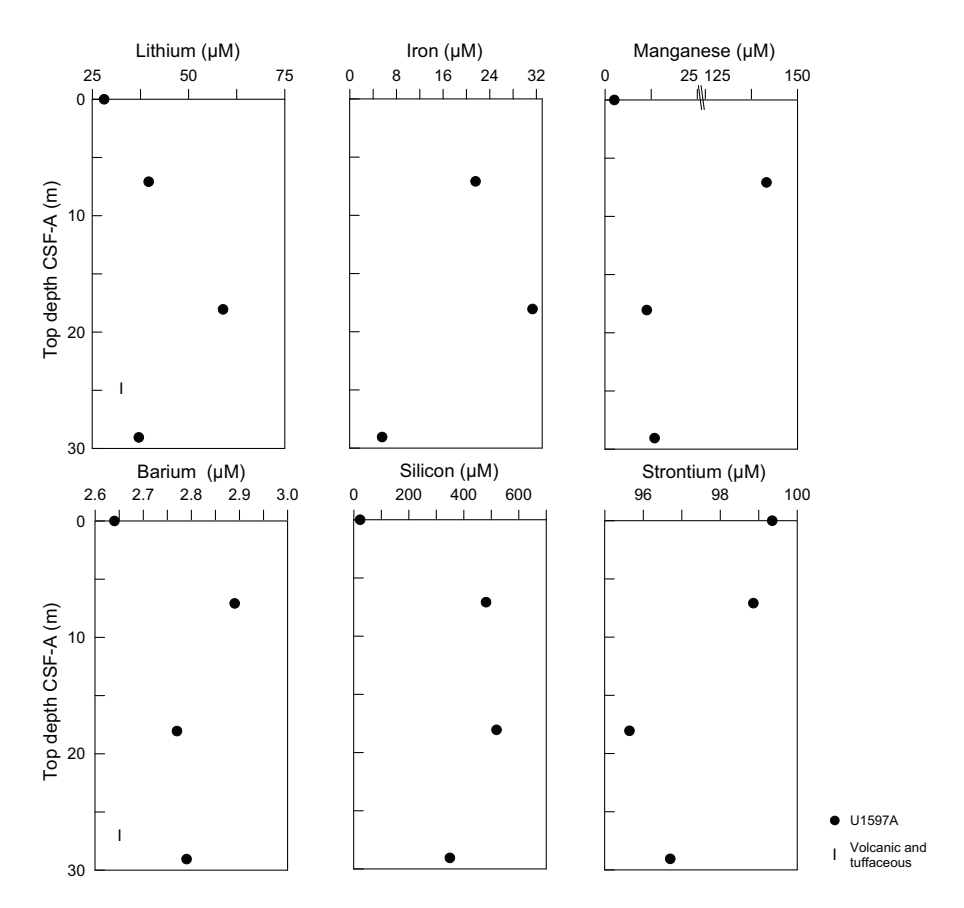


Figure F16. ICP-AES concentrations of Li, Fe, Mn, Ba, Si, and Sr in IW samples, Site U1597. Lithostratigraphic Unit I is described in Lithostratigraphy.

Table T11. Total inorganic carbon (TIC), percent CaCO₃, TC, total nitrogen (TN), and TOC data, Site U1597. **Download table in CSV format.**

9.4. Headspace gas analysis

Headspace gas analyses were performed at a resolution of one sample per full-length core (9.5 m advance) throughout Hole U1597A. The aim was to monitor the presence and abundance of C_1 – C_3 hydrocarbons as part of the standard International Ocean Discovery Program safety protocol (Pimmel and Claypool, 2001). A total of nine headspace gas samples from this hole were analyzed using gas chromatography (GC) (see **Geochemistry** in the Expedition 398 methods chapter [Kutterolf et al., 2024]). Methane, ethane, and propane concentrations were below the detection limit throughout Hole U1597A. Concentrations of heavier hydrocarbons (*iso*-butane, *n*-butane, and *n*-pentane, etc.) were below the detection limit throughout Hole U1597A.

References

Druitt, T., Kutterolf, S., and Höfig, T.W., 2022. Expedition 398 Scientific Prospectus: Hellenic Arc Volcanic Field. International Ocean Discovery Program. https://doi.org/10.14379/iodp.sp.398.2022

Druitt, T.H., Kutterolf, S., Ronge, T.A., Beethe, S., Bernard, A., Berthod, C., Chen, H., Chiyonobu, S., Clark, A., DeBari, S., Fernandez Perez, T.I., Gertisser, R., Hübscher, C., Johnston, R.M., Jones, C., Joshi, K.B., Kletetschka, G., Koukousioura, O., Li, X., Manga, M., McCanta, M., McIntosh, I., Morris, A., Nomikou, P., Pank, K., Peccia, A., Polymenakou, P.N., Preine, J., Tominaga, M., Woodhouse, A., and Yamamoto, Y., 2024. Site U1589. In Druitt, T.H., Kutterolf, S., Ronge, T.A., and the Expedition 398 Scientists, Hellenic Arc Volcanic Field. Proceedings of the International Ocean Discovery Program, 398: College Station, TX (International Ocean Discovery Program). https://doi.org/10.14379/iodp.proc.398.103.2024

- Fisher, R.V., and Schmincke, H.-U., 1984. Pyroclastic Rocks: Berlin (Springer). https://doi.org/10.1007/978-3-642-74864-6
- Johnston, E.N., Sparks, R.S.J., Nomikou, P., Livanos, I., Carey, S., Phillips, J.C., and Sigurdsson, H., 2015. Stratigraphic relations of Santorini's intracaldera fill and implications for the rate of post-caldera volcanism. Journal of the Geological Society (London, UK), 172(3):323–335. https://doi.org/10.1144/jgs2013-114
- Jutzeler, M., White, J.D.L., Talling, P.J., McCanta, M., Morgan, S., Le Friant, A., and Ishizuka, O., 2014. Coring disturbances in IODP piston cores with implications for offshore record of volcanic events and the Missoula megafloods. Geochemistry, Geophysics, Geosystems, 15(9):3572–3590. https://doi.org/10.1002/2014GC005447
- Kidd, R.B., Cita, M.B., and Ryan, W.B.F., 1978. Stratigraphy of eastern Mediterranean sapropel sequences recovered during DSDP Leg 42A and their paleoenvironmental significance. In Hsü, K., Montadert, L., et al., Initial Reports of the Deep Sea Drilling Project. 42(1): Washington, DC (US Government Printing Office), 421–443. https://doi.org/10.2973/dsdp.proc.42-1.113-1.1978
- Kutterolf, S., Druitt, T.H., Ronge, T.A., Beethe, S., Bernard, A., Berthod, C., Chen, H., Chiyonobu, S., Clark, A., DeBari, S., Fernandez Perez, T.I., Gertisser, R., Hübscher, C., Johnston, R.M., Jones, C., Joshi, K.B., Kletetschka, G., Koukousioura, O., Li, X., Manga, M., McCanta, M., McIntosh, I., Morris, A., Nomikou, P., Pank, K., Peccia, A., Polymenakou, P.N., Preine, J., Tominaga, M., Woodhouse, A., and Yamamoto, Y., 2024. Expedition 398 methods. In Druitt, T.H., Kutterolf, S., Ronge, T.A., and the Expedition 398 Scientists, Hellenic Arc Volcanic Field. Proceedings of the International Ocean Discovery Program, 398: College Station, TX (International Ocean Discovery Program). https://doi.org/10.14379/iodp.proc.398.102.2024
- Kutterolf, S., Freundt, A., Hansteen, T.H., Dettbarn, R., Hampel, F., Sievers, C., Wittig, C., Allen, S.R., Druitt, T.H., McPhie, J., Nomikou, P., Pank, K., Schindlbeck-Belo, J.C., Wang, K.-L., Lee, H.-Y., and Friedrichs, B., 2021. The medial offshore record of explosive volcanism along the central to eastern Aegean Volcanic Arc: 1. tephrostratigraphic correlations. Geochemistry, Geophysics, Geosystems, 22(12):e2021GC010010. https://doi.org/10.1029/2021GC010010
- Le Maitre, R.W., Steckeisen, A., Zanettin, B., Le Bas, M.J., Bonin, B., and Bateman, P. (Eds.), 2002. Igneous Rocks: A Classification and Glossary of Terms (Second edition): Cambridge, UK (Cambridge University Press). https://doi.org/10.1017/CBO9780511535581
- Nomikou, P., Druitt, T.H., Hübscher, C., Mather, T.A., Paulatto, M., Kalnins, L.M., Kelfoun, K., Papanikolaou, D., Bejelou, K., Lampridou, D., Pyle, D.M., Carey, S., Watts, A.B., Weiß, B., and Parks, M.M., 2016. Post-eruptive flooding of Santorini caldera and implications for tsunami generation. Nature Communications, 7(1):13332. https://doi.org/10.1038/ncomms13332
- Pimmel, A., and Claypool, G., 2001. Introduction to shipboard organic geochemistry on the JOIDES Resolution. Ocean Drilling Program Technical Note, 30. https://doi.org/10.2973/odp.tn.30.2001